HHS Public Access

Author manuscript

Cell Rep. Author manuscript; available in PMC 2022 January 01.

Published in final edited form as:

Cell Rep. 2021 December 07; 37(10): 110085. doi:10.1016/j.celrep.2021.110085.

SOX10 requirement for melanoma tumor growth is due, in part, to immune-mediated effects

Sheera R. Rosenbaum[1], **Manoela Tiago**[1], **Signe Caksa**[1], **Claudia Capparelli**[1,2], **Timothy J. Purwin**[1], **Gaurav Kumar**[1], **McKenna Glasheen**[1], **Danielle Pomante**[1], **Daniel Kotas**[1], **Inna Chervoneva**[3], **Andrew E. Aplin**[1,2,4,*]

[1]Department of Cancer Biology, Thomas Jefferson University, Philadelphia, PA 19107, USA

[2]Sidney Kimmel Cancer Center, Thomas Jefferson University, Philadelphia, PA 19107, USA

[3]Division of Biostatistics in the Department of Pharmacology and Experimental Therapeutics, Thomas Jefferson University, Philadelphia, PA 19107, USA

[4]Lead contact

SUMMARY

Developmental factors may regulate the expression of immune modulatory proteins in cancer, linking embryonic development and cancer cell immune evasion. This is particularly relevant in melanoma because immune checkpoint inhibitors are commonly used in the clinic. SRY-box transcription factor 10 (SOX10) mediates neural crest development and is required for melanoma cell growth. In this study, we investigate immune-related targets of SOX10 and observe positive regulation of herpesvirus entry mediator (HVEM) and carcinoembryonic-antigen cell-adhesion molecule 1 (CEACAM1). *Sox10* knockout reduces tumor growth in vivo, and this effect is exacerbated in immune-competent models. Modulation of CEACAM1 expression but not HVEM elicits modest effects on tumor growth. Importantly, *Sox10* knockout effects on tumor growth are dependent, in part, on CD8+ T cells. Extending this analysis to samples from patients with cutaneous melanoma, we observe a negative correlation with SOX10 and immune-related

*Correspondence: andrew.aplin@jefferson.edu.

AUTHOR CONTRIBUTIONS

S.R.R., C.C., and A.E.A. conceived the study. S.R.R. and A.E.A. designed the experiments and analyzed the data. M.T. contributed to the completion of *in vivo* experiments. C.C. generated the MeWo *SOX10* knockout cells and RNA-seq dataset, which was analyzed by G.K. S.C. and D.K. performed genomic validation of *SOX10* knockout. S.C. and M.G. completed SOX10 re-expression studies. D.P. and M.G. completed characterization of mouse melanoma cell lines. T.J.P. contributed the correlation analyses of lymphocyte scores and mRNA, performed analysis of ATAC-seq data, and advised on other TCGA correlation analyses. G.K. processed and analyzed YUMM1.1 RNA-seq data. I.C. performed the zero-inflated negative binomial regression modeling of single-cell RNA-seq data. All other experiments and analyses were performed by S.R.R. S.R.R. and A.E.A. wrote the manuscript.

DECLARATION OF INTERESTS

A.E.A. reports receiving a commercial research grant from Pfizer Inc. (2013–2017) and has ownership interest in patent number 9880150. No potential conflicts of interest were disclosed by the other authors.

SUPPLEMENTAL INFORMATION

Supplemental information can be found online at https://doi.org/10.1016/j.celrep.2021.110085.

INCLUSION AND DIVERSITY

We worked to ensure diversity in experimental samples through the selection of the cell lines. We worked to ensure diversity in experimental samples through the selection of the genomic datasets. One or more of the authors of this paper self-identifies as an underrepresented ethnic minority in science.

pathways. These data demonstrate a role for SOX10 in regulating immune checkpoint protein expression and anti-tumor immunity in melanoma.

In brief

SOX10 is a lineage-specific transcription factor that facilitates neural crest cell development and contributes to melanoma cell growth. Rosenbaum et al. investigate potential immune-related roles for SOX10 in melanoma. They observe that *Sox10* knockout reduces expression of the immune checkpoint proteins HVEM and CEACAM1 and mediates effects on tumor growth in immune-competent models.

Graphical Abstract

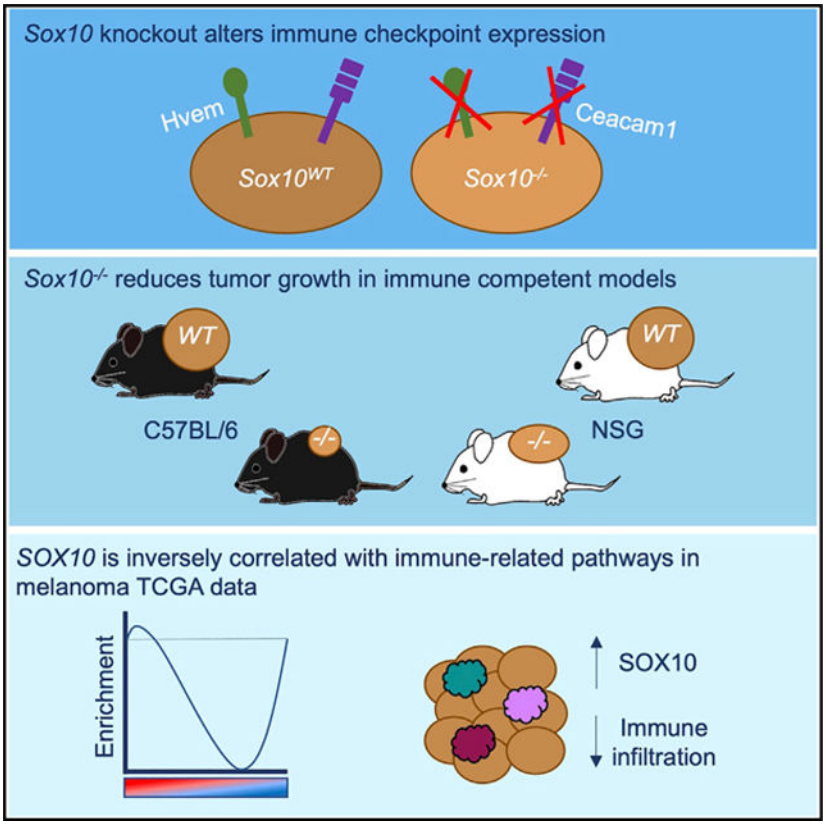

INTRODUCTION

During embryonic development, neural crest cells migrate and differentiate into numerous cell types, including neurons of the peripheral nervous system, smooth muscle cells of the cardiovascular system, and pigment cells of the skin. Developmental processes are tightly controlled by the temporal and tissue-specific expression of a network of key transcription factors. Melanocytes are pigmented cells and their differentiation is largely dependent on the expression of SRY-box transcription factor 10 (SOX10) and melanocyte-inducing transcription factor (MITF). The transformation of melanocytes gives rise to melanoma, and SOX10 expression in melanoma cells promotes proliferation, tumor formation, and growth

(Cronin et al., 2013; Shakhova et al., 2012). In contrast, the loss of SOX10 is associated with resistance to BRAF-targeted inhibitors (Sun et al., 2014). Thus, although SOX10 initially promotes melanoma growth, it may play different roles in resistant tumors.

In fetal development, immune checkpoint proteins, inflammatory mediators, and major histocompatibility (MHC) proteins play important roles in promoting immunotolerance at the maternal-fetal interface (Kanellopoulos-Langevin et al., 2003; Miko et al., 2019; Tersigni et al., 2020). Several studies have demonstrated a link between embryonic transcription factors and the expression of immune modulatory proteins. The early embryonic transcription factor double homeobox 4 (DUX4) negatively regulated the expression of MHC class I proteins and was associated with reduced survival in response to immune checkpoint blockade in cutaneous melanoma (Chew et al., 2019). In a mouse model of melanoma, the transcription factor Snail, which promotes the epithelial-to-mesenchymal transition (EMT) during embryonic development, promoted immunosuppression through upregulation of the angiogenic protein thrombospondin-1 (TSP-1) (Kudo-Saito et al., 2009). In breast cancer, positive regulation of the immune checkpoint programmed death-ligand 1 (PD-L1) by the developmental regulator Eya3 promoted tumor growth (Vartuli et al., 2018). We also recently demonstrated that the embryonic transcription factor FOXD3 regulates expression of the immune checkpoint VISTA in melanoma (Rosenbaum et al., 2020). Immune checkpoint proteins fine-tune the anti-tumor immune response and regulate the ability of cancer cells to escape immune surveillance and attack from CD8+ T cells. Furthermore, these proteins are commonly targeted in the clinic. Immune checkpoint inhibitors targeting cytotoxic lymphocyte-associated protein 4 (CTLA-4) or programmed cell death 1 (PD-1) have been approved by the US Food and Drug Administration (FDA) for the treatment of cutaneous melanoma. Although immune checkpoint inhibitors improve survival and response durability for patients with melanoma, many tumors still do not respond to these therapies, prompting the investigation of alternative immune-related targets.

Although it is evident that there are connections between embryonic development and cancer, a thorough understanding of the role of developmental regulators in modulating anti-tumor immunity is lacking. Given that SOX10 is a critical regulator of melanocytic development and melanoma cell growth, we tested whether SOX10 regulates immune-related targets in melanoma. We observed that SOX10 regulates expression of the immune checkpoint proteins herpesvirus entry mediator (HVEM) and carcinoembryonic-antigen cell-adhesion molecule 1 (CEACAM1) and that *Sox10* ablation decreases tumor growth in immune-competent models in a T-cell-dependent manner. Overall, we offer insight into the role of SOX10 in promoting melanoma tumor growth and provide evidence that it regulates multiple immune checkpoint proteins in melanoma.

RESULTS

Immune checkpoints CEACAM1 and HVEM are downstream targets of the SOX10 regulatory network

To understand the role of SOX 10 inanti-tumorimmunity, we investigated the regulation of potential immune-related targets. We used CRISPR-Cas9 to knockout expression of *Sox10* in the $Braf^{V600E}Cdkn2a^{-/-}Pten^{-/-}$ mouse melanoma cell line YUMM1.1 (Meeth

et al., 2016). We chose this mouse cell line because it was generated with genetic alterations that resemble driver mutations in human melanoma (Meeth et al., 2016) and shows a high expression of SOX10 (Figure S1A). Compared to other mouse melanoma cell lines, YUMM1.1 showed equivalent levels of the pigmentation protein tyrosinase but low expression of other pigmentation proteins such as gp100 and Mitf(Figure S1A). Two independent *Sox10* knockout clones were generated (referred to as CR. #1.41 and CR. #1.51), and *Sox10* knockout was verified by western blot (Figure 1A) and by sequencing of genomic DNA at regions targeted by *Sox10* guide RNA (Figure S1B). CRISPR-Cas9 was also used to knockout the expression of *SOX10* in the *BRAF* wild-type human melanoma cell line MeWo (full details in C.C., unpublished data), and *SOX10* knockout was verified by western blot (Figure 1B) and by sequencing of genomic DNA (Figure S1B). We next performed RNA sequencing (RNA-seq) analysis comparing parental cells with *Sox10* knockout cells (BioProject: PRJNA688784; BioProject: PRJNA701949) and analyzed path way alterations by gene set enrichment analysis (GSEA)(Table S1). This analysis did not support an immune-related signature, which is not surprising considering the multifaceted role of SOX10 in melanoma. Given the translational relevance of immune checkpoint proteins, we mined the datasets for alterations across a panel of immune modulatory proteins (Figures 1C and 1D). We selected immune modulatory proteins for further study based on fold changes that were significant and comparable between the two models. Based on this selection, we identified SOX10-depdent alterations in Galectin-9 (Gal-9; *LGALS9*), HVEM (*TNFRSF14*), cluster of differentiation 47 (CD47; *CD47*), PD-L1 (*CD274*), and CEACAM1 (*CEACAM1*).

We next sought to validate the expression of Gal-9, CD47, PD-L1, HVEM, and CEACAM1 at the protein level. Ananalysis was performed in both the absence and presence of interferon-$_{\gamma}$ (IFN$_{\gamma}$), which is known to induce PD-L1 expression (Garcia-Diaz et al., 2017). We did not detect basal or IFN$_{\gamma}$-inducible expression of Gal-9 in YUMM1.1 cells (Figure S1C). PD-L1 was not expressed basally in YUMM1.1, and IFN$_{\gamma}$ induction of PD-L1 was not altered in *Sox10* knockout cells (Figure S1D). CD47 was detectable but not consistently altered in MeWo *SOX10* knockout cells and expressed at low levels in YUMM1.1 cells (Figures S1E and S1F).

In contrast to Gal-9, CD47, and PD-L1, we observed SOX10-dependent regulation of HVEM and CEACAM1. HVEM and CEACAM1 transcript levels were markedly altered in *Sox10* knockout cells within the RNA-seq dataset compared to other genes (Figure 1E). Cell surface expression of HVEM was IFN$_{\gamma}$ inducible in mouse YUMM1.1 parental cells; *Sox10* ablation reduced IFN$_{\gamma}$-inducible but not basal HVEM levels (Figure 2A). Human MeWo parental cells displayed high basal levels of HVEM, and *SOX10* ablation reduced both basal and IFN$_{\gamma}$-inducible expression (Figure 2B). Cell surface expression of CEACAM1 was not IFN$_{\gamma}$ inducible, and basal levels were reduced in YUMM1.1 *Sox10* knockout cells (Figure 2C). In human MeWo parental cells, CEACAM1 was IFN$_{\gamma}$ inducible and levels were reduced in *SOX10* knockout cells (Figure 2D). CEACAM1 is heavily glycosylated and alternatively spliced as short and long isoforms (Gray-Owen and Blumberg, 2006; Houde et al., 2003). To visualize CEACAM1 expression with associated glycosylation changes in parental and *Sox10* knockout cells, we performed western blotting. In mouse YUMM1.1 cells, expression of both high- and low-molecular-weight isoforms of CEACAM1 was

reduced in *Sox10* knockout cells (Figure 2E; Figure S2A). In human MeWo cells, only high-molecular-weight isoforms of CEACAM1 were expressed, and both endogenous and IFN_{γ}-inducible CEACAM1 expression were reduced in *SOX10* knockout cells (Figure 2F; Figure S2B). Transient knockdown of *Sox10* in additional mouse melanoma (B16F10) and human melanoma (SKMel28 and SKMel30) cell lines also showed that CEACAM1 expression was SOX10dependent (Figures S2C–S2E). Lastly, re-expression of SOX10 partially rescued the expression of CEACAM1 in YUMM1.1 CR. *Sox10* #1.41 cells and in MeWo CR. *SOX10* #4.11 cells (Figures S2F and S2G) and had a modest effect on cell surface expression of HVEM in MeWo CR. *SOX10* #4.11 cells (Figure S2H).

To further interrogate the relationship between SOX10 and CEACAM1 and HVEM, we analyzed data from a publicly available study (GEO: GSE114557) containing assay for transposase-accessible chromatin using sequencing (ATAC-seq) analysis on samples from patients with melanoma after *SOX10* knockdown (Bravo González-Blas et al., 2019). We observed regions of open chromatin surrounding the transcription start site of *CEACAM1* and at the transcription start site of *TNFRSF14* (gene name for HVEM), which significantly decreased upon *SOX10* knockdown (Table S2), suggesting that SOX10 may modulate the chromatin accessibility of these genes. Although these data provide evidence that CEACAM1 and HVEM are a part of the larger regulatory network controlled by SOX10, whether or not they are direct targets of SOX10 remains to be established in future studies. Altogether, these data identify HVEM and CEACAM1 as putative targets of the SOX10 regulatory network.

SOX10 expression is positively correlated with CEACAM1 and HVEM in sample datasets from patients with melanoma

To extend the analysis of SOX10 regulation of immune checkpoint proteins, we analyzed patient sample databases (Cerami et al., 2012; Gao et al., 2013). When we compared datasets from The Cancer Genome Atlas (TCGA) across cancer types, SOX10, HVEM, and CEACAM1 were highly expressed in cutaneous melanoma compared to other cancers (Figure S3). Furthermore, within the cutaneous melanoma TCGA dataset (Cerami et al., 2012; Gao et al., 2013), SOX10 mRNA levels were moderately correlated with HVEM mRNA levels (Spearman = 0.33) and CEACAM1 mRNA levels (Spearman = 0.17) (Figures 3A and 3B). Because the bulk RNA-seq data from TCGA are derived from tumor samples containing some stromal components, we used publicly available single-cell RNA-seq data of tumors from patients with melanoma (Jerby-Arnon et al., 2018) to evaluate the expression of HVEM and CEACAM1 compared to SOX10 specifically in malignant cells at the single-cell level (Figure 3C). We observed heterogenous expression of all three targets within tumors but that the two SOX10-negative tumors also lacked expression of both HVEM and CEACAM1. We applied a zero-inflated negative binomial regression model to quantitatively evaluate the dependency of HVEM and CEACAM1 expression on SOX10 expression in this dataset. We observed a statistically significant association in the expression of HVEM and SOX10, reflected as an odds ratio of <1 and a positive mean difference, but the association between CEACAM1 and SOX10 was not significant (Figure S3D). These results suggest that the expression of SOX10 correlates with HVEM in samples from patients with

melanoma. The weaker correlation between SOX10 and CEACAM1 suggests that additional mechanisms may control CEACAM1 in melanoma cells.

Sox10 ablation decreases tumor growth and extends survival in immune-competent models

Given the multiple effects of SOX10 on immune modulatory proteins, we investigated immune-dependent effects of SOX10 in melanoma. We evaluated effects of *Sox10* knockout on *in vitro* proliferation and observed a decrease in cell growth (Figures 4A and 4B). Next, we intradermally injected parental and *Sox10* knockout cells into either severely immune-deficient NOD.*Cg-Prkdc*^{scid}*IL2rg*^{tm1Wjl}*/SzJ* (NSG) mice or immune-competent C57BL/6 (BL6) mice and monitored tumor growth. In the immune-deficient NSG mouse model, we observed modest effects on tumor growth and survival in one of the two *Sox10* knockout clones compared to parental cells (Figures 4C and 4D). In immune-competent BL6 mice, we observed striking effects of *Sox10* knockout on tumor growth and survival (Figures 4E and 4F). Only 3/5 (60%) mice injected with CR. *Sox10* #1.41 formed tumors, with delayed growth for the other two tumors (Figure 4E). Similarly, with CR. *Sox10* #1.51, only 1/5 (20%) tumors formed, and this mouse was sacrificed early due to tumor necrosis (Figure 4E). We used a second mouse melanoma model, 1014 cells, which harbors a human-relevant *NRAS* mutation (Petit et al., 2019) and expresses high levels of SOX10 (Figure S1A). Using CRISPR-Cas9, we generated two independent *Sox10* knockout clones, verified *Sox10* knockout by western blot, and observed similar effects on CEACAM1 expression in these cells (Figure S4A). In immune-competent BL6 mice, we observed similar effects of *Sox10* knockout in delaying tumor growth and extending survival (Figures S4B–S4D). These findings indicate that *Sox10* knockout reduces tumor growth and that this effect is exacerbated in immune-competent models.

Modulating expression of individual immune checkpoints alone has moderate effects on tumor growth in immune-competent models

We identified HVEM and CEACAM1 as putative immune-related targets of SOX10. First, we tested the ability of HVEM re-expression to rescue effects of *Sox10* ablation on tumor growth. To this end, we engineered YUMM1.1 CR. *Sox10* #1.41 knockout cells to overexpress HVEM and validated HVEM expression by flow cytometry staining (Figure 5A). Notably, HVEM levels in overexpressing cells were comparable to IFN$_\gamma$-inducible HVEM levels in parental cells (Figure S4E). Next, we tracked tumor growth of HVEM-overexpressing tumors. We observed no difference in tumor growth of HVEM-overexpressing tumors compared with that of parental YUMM1.1 cells, and HVEM overexpression did not rescue tumor growth effects of CR. *Sox10* #1.41 knockout cells (Figure 5B). Consistent with these effects, HVEM expression did not alter time-to-tumor onset, defined as reaching a tumor volume of ~50 mm^3 (Figure 5C).

We next tested the effect of CEACAM1 on tumor growth. Because CEACAM1 can be found in numerous isoforms, either short or long, glycosylated or non-glycosylated, we used a CRISPR-Cas9 knockout approach to study the effects of this immune checkpoint. Two independent *Ceacam1* knockout clones were generated, and *Ceacam1* ablation was verified by flow cytometry and western blot (Figure 5D; Figure S4F). In tumor growth assays, we

observed moderate effects of *Ceacam1* knockout on tumor growth and time to tumor onset (Figures 5E and 5F); however, effects of *Ceacam1* knockout on tumor growth were not comparable to the effects of *Sox10* knockout (Figures 4E and 4F). These findings suggest a contribution of CEACAM1 to immune-related effects, although it is clear that modulation of individual SOX10-regulated immune targets alone does not sufficiently emulate the effects of *Sox10* ablation on tumor growth in immune-competent models.

Immune-dependent effects of *Sox10* ablation on tumor growth are mediated, in part, by T cells

Multiple immune cell types are either absent or defective in NSG mice, including B cells, T cells, dendritic cells, macrophages, and natural killer (NK) cells. Any of these immune cell types might be responsible for controlling the growth of *Sox10* knockout tumors. We interrogated the contribution of individual immune cell populations to the immune-dependent effects of *Sox10* ablation on tumor growth. To this end, we injected parental or *Sox10* knockout cells into B6.129S7-*Rag1*^{tm1Mom}/J (*Rag1* KO) mice, which are lacking in B and T cells. In comparison to parental cells, CR. *Sox10* #1.51 had a delay in tumor growth in *Rag1* KO mice (Figure 6A). However, CR. *Sox10* #1.51 tumors formed more frequently and significantly faster in *Rag1* KO mice than immune-competent BL6 mice (Figures 6B and 6C). Furthermore, we observed decreased survival in *Rag1* KO mice compared with that of immune-competent BL6 mice (Figure 6D). A similar trend was observed with CR. *Sox10* #1.41 cells, namely, 100% (5/5) of tumors formed in *Rag1* KO mice compared to 60% (3/ 5) of tumors in BL6 mice (Figures 4E and S5).

Rag1 KO mice lack both CD8+ and CD4+ T cells in addition to lacking B cells. Because CD8+ T cells play an important role in the elimination of cancer cells, we treated BL6 mice with an anti-mouse CD8α antibody (clone 53–6.72) to specifically deplete CD8+ T cells or treated mice with an isotype control. Mice were injected intradermally with parental or *Sox10* knockout cells, and tumor growth was monitored. CR. *Sox10* #1.51 formed tumors more frequently and significantly faster in CD8+-depleted mice than mice treated with the isotype control (Figures 6B and 6C). We observed a trend toward decreased survival in CD8+-depleted mice (Figure 6D); however, this result was not statistically significant. Of note, in both CR. *Sox10* #1.51 and CR. *Sox10* #1.41 experiments, the isotype control exerted effects on tumor formation and growth, which were exaggerated in CR. *Sox10* #1.41 tumors (Figures 6B–6D; Figures S5B–S5D). The absence or depletion of T cells was verified in *Rag1* KO (Figures S6A and S6B) and CD8+ T cell depletion experiments (Figures S6C and S6D) by flow cytometry staining. These results demonstrate that the effects of *Sox10* ablation on tumor growth are mediated in part by CD8+ T cells.

SOX10 is inversely correlated with immune-related gene pathways in melanoma

To broadly evaluate the relationship between SOX10 mRNA expression and immune cell infiltration, we used a TCGA dataset of cutaneous melanoma (Cancer Genome Atlas Network, 2015). Each patient sample in the melanoma TCGA dataset has been evaluated by immunohistochemistry for lymphocyte distribution and density, and these two values were summed together, resulting in a lymphocyte score (Lscore). We observed that the SOX10 mRNA level is inversely correlated with this Lscore in melanoma in a statistically

significant manner (Figure 7A). Because SOX10 is highly expressed in melanoma cells, we also evaluated the relationship of other melanoma-expressed genes with immune infiltration. In contrast to *SOX10*, other pigment-related melanoma-expressed genes, such as *MCAM*, *S100A1*, and *MLANA*, showed a markedly weaker correlation with immune cell infiltration (Figure S7A). Next, we performed GSEA on TCGA data of SOX10 mRNA expression to determine enriched pathways in the Kyoto Encyclopedia of Genes and Genomes (KEGG) gene set collection. Multiple metabolism-related pathways positively correlated with SOX10, including oxidative phosphorylation, amino sugar nucleotide sugar metabolism, and pentose phosphate pathway (Figure S7B). Most significantly enriched pathways found to be negatively correlated with SOX10 expression were associated with immune-related pathways (Figure 7B). Interestingly, pathways involved in NK cell cytotoxicity and T cell receptor signaling were among the top enriched pathways found to be negatively correlated with SOX10 expression (Figures 7B and 7C). In contrast, the pigment-related, melanoma-expressed genes *MLANA* and *MCAM* were enriched for very few immune-related gene pathways, and *MLANA* was not negatively correlated with pathways for NK cell cytotoxicity or T cell receptor signaling (Figures S7C and S7D). These data are consistent with our preclinical findings and indicate that SOX10 is negatively correlated with several immune-related pathways in samples from patients with melanoma.

DISCUSSION

SOX10 is known to be required for tumor formation and melanoma cell growth; however, its role in modulating tumor-immune interactions is poorly understood. In this study, we investigated immune-related roles of SOX10. We identified two putative targets, namely, HVEM and CEACAM1, and showed that SOX10 effects on melanoma growth are dependent, in part, on an intact immune system. SOX10 effects were partially mediated by CD8+ T cells; however, modulating expression of HVEM and CEACAM1 individually did not completely emulate effects of *Sox10* knockout on tumor formation and growth. In sample databases from patients with cutaneous melanoma, SOX10 was negatively correlated with immune infiltrates and immune-related pathways. Thus, the ability of SOX10 to promote melanomagenesis may be, in part, due to its regulation of immune-related targets.

We show that *SOX10* knockout reduces the expression of the immune checkpoints HVEM and CEACAM1 in melanoma cells. It is important to note that although HVEM was constitutively expressed in MeWo cells, IFN_{γ} stimulation was required to detect HVEM in YUMM1.1 cells, resembling the heterogeneous IFN_{γ}-inducible patterns of PD-L1 expression observed in cancer cells (Atefi et al., 2014; Thiem et al., 2019). The mechanism by which SOX10 regulates these genes requires further investigation. Although SOX10 can regulate genes by binding to the promoter or to distal enhancers (Fufa et al., 2015), other mechanisms could be also involved. Using publicly available ATAC-seq data (Bravo González-Blas et al., 2019), we observed that areas of open chromatin surrounding the *CEACAM1* and *TNFRSF14* gene loci are reduced following *SOX10* knockdown, suggesting that SOX10 may regulate these genes at the chromatin level. Previous studies have also shown that CEACAM1 may be indirectly regulated by the related SOX family member SOX9 (Ashkenazi et al., 2016; Zalzali et al., 2008). Furthermore, the SOX10-regulated protein MITF has been reported to modulate HVEM expression (Malissen et al., 2019).

Thus, although HVEM and CEACAM1 are controlled by the SOX10 regulatory network, the exact mechanism of regulation requires further investigation.

We observed that HVEM re-expression was not sufficient to rescue the effects of *Sox10* ablation on tumor growth. HVEM interacts with multiple inhibitory and stimulatory ligands and receptors to modulate T cell function, acting as a molecular switch for T cell co-stimulation (Murphy et al., 2006; Rodriguez-Barbosa et al., 2019). Its engagement with the receptors BTLA and CD160 on T cells inhibits T cell function (Cai et al., 2008; Sedy et al., 2005; Zhang et al., 2016), and expression of HVEM and BTLA have been associated with poor prognosis in several cancers (Inoue et al., 2015; Lan et al., 2017; Tang et al., 2019). Alternatively, HVEM engagement with the protein LIGHT triggers bidirectional stimulatory signaling that has been shown to promote T cell proliferation and activation or apoptosis in a context-dependent manner (Mortarini et al., 2005; Rodriguez-Barbosa et al., 2019; Tamada et al., 2000). Thus, the role of HVEM in cancer is not yet thoroughly understood, and its net effect on anti-tumor immunity may depend on the expression of stimulatory and inhibitory receptors on immune cells in the tumor microenvironment.

CEACAM1 serves roles in cell-cell adhesion, invasion, metabolism, and immune modulation (Gray-Owen and Blumberg, 2006) and may be a prognostic indicator of melanoma progression and metastasis (Dankner et al., 2017). CEACAM1 modulates T cell activity either through homophilic interactions or interactions with the inhibitory receptor TIM-3, igniting interest in CEACAM1 as a potential immunotherapy target (Huang et al., 2015). We observed that expression of CEACAM1 had moderate effects on tumor formation, which is consistent with reports that CEACAM1 silencing reduces tumor growth in melanoma and colon cancer models (Chen et al., 2011; Wicklein et al., 2018). These tumor growth effects have been attributed both to the role of CEACAM1 in modulating anti-tumor immune responses and in performing tumor intrinsic functions. The role of CEACAM1 in cancer is controversial, with several reports showing that CEACAM1 may promote tumor progression and others demonstrating that it acts as a tumor suppressor (Sienel et al., 2003; Takeuchi et al., 2019; Thies et al., 2002). CEACAM1 is alternatively spliced into 12 different isoforms that are primarily defined by the number of C2-like immunoglobulin (Ig) domains in the extracellular region and by the length of the cytoplasmic domain, namely, long (CEACAM1-L) or short (CEACAM1-S) (Dankner et al., 2017). Furthermore, CEACAM1 is heavily posttranslationally modified by N-linked glycosylation (Houde et al., 2003). In tumor cells, knockdown studies demonstrated that tumor-specific expression of CEACAM1 inhibits specific lysis by T cells and NK cells (Chen et al., 2011; Markel et al., 2002, 2009). However, another study found that the specific expression of the 3S isoform in tumor cells, but not other isoforms, promotes NK-cell-mediated lysis (Ullrich et al., 2015). Alternative roles for long and short isoforms are also observed in T cells and NK cells in which the long isoform predominates and acts as an inhibitory receptor, whereas the short isoform acts as a costimulatory receptor (Chen et al., 2004). Thus, the controversy surrounding the role of CEACAM1 in cancer may be the result of complex splicing patterns and the context-specific expression of CEACAM1 isoforms. For this reason, in our studies, we used a knockout approach to focus on the endogenous role of CEACAM1 in tumor formation. Future studies should further address the differential roles of CEACAM1 isoforms in modulating anti-tumor immunity.

SOX10 executes tumor intrinsic functions, and consistent with previous publications (Cronin et al., 2013; Shakhova et al., 2012), its knockout reduced cell proliferation of mouse melanoma cells *in vitro* and tumor growth *in vivo* in immune-deficient mice. In immune-competent mice, SOX10 effects on tumor growth were exacerbated, and this effect was partially dependent on CD8+ T cells, suggesting a role for an intact immune system. Although CD8+ T cells are major effectors of anti-tumor immunity, there are many other immune cell types that contribute to immune surveillance and immune cell killing. NK cells play a crucial role in eliminating cancer cells during tumorigenesis (Huntington et al., 2020). The role of B cells in cancer is not yet fully understood, with studies showing either pro- or anti-tumorigenic roles (Largeot et al., 2019). This is especially relevant to the study of CEACAM1 and HVEM because these checkpoints have been demonstrated to exert effects not only on T cells but also on NK cells and B cells (Chen et al., 2011; Mintz et al., 2019; Ullrich et al., 2015). Furthermore, macrophages play both pro- and anti-tumorigenic roles and can modulate the activity and infiltration of T cells (Pathria et al., 2019). Thus, although we observed a partial dependency of SOX10 effects on CD8+ T cells, other immune cell types are likely involved in melanoma tumorigenesis.

The role of SOX10 in melanoma is multi-faceted. SOX10 is required for the formation of melanoma tumors by regulating a “proliferative” state (Shakhova et al., 2012; Verfaillie et al., 2015). Altered expression of SOX10 has been associated with tumor cell plasticity and phenotype switching. Specifically, the loss of SOX10 expression is associated with a switch to a de-differentiated, mesenchymal phenotype that promotes invasion and resistance to targeted therapy (Rambow et al., 2018, 2019; Sun et al., 2014; Verfaillie et al., 2015; Wouters et al., 2020). This result is supported by ATAC-seq studies in melanoma that observed an increase in chromatin accessibility at mesenchymal-like genes and a collapse of melanocytic gene regions upon *SOX10* knockdown, providing evidence that SOX10 may modulate global gene expression through epigenetic mechanisms (Bravo González-Blas et al., 2019; Wouters et al., 2020). Although SOX10 positively regulates tumor growth and formation, its effect on cell phenotype suggests that it may play a different role in metastasis and therapeutic resistance. We did not observe a phenotype switch as a result of *Sox10* knockout (data not shown), and we recognize that a limitation of mouse models is that they imperfectly recapitulate the high degree of heterogeneity in melanoma. Recent work has developed additional melanoma mouse models with differences in basal differentiation status, which will have important implications for the study of phenotype switching and tumor cell plasticity (Pérez-Guijarro et al., 2020). Nonetheless, an advantage of *Sox10* loss in the YUMM1.1 syngeneic mouse melanoma model is that it permits the study of effects on anti-tumor immunity in the absence of phenotypic alterations. Importantly, we have validated our findings in human melanoma cell models and patient samples. Future studies should address the effect of SOX10-related phenotype switching on anti-tumor immune responses.

Limitations of the study

There are several limitations to the experiments conducted in this study. Given that *Sox10*-deficient cells either did not form tumors or formed tumors at a much later time point than parental cells, we were not able to collect tumors at early time points for the analysis of

tumor-infiltrating lymphocytes. This issue may be addressed in the future by using models that allow for inducible knockdown of *Sox10*. Furthermore, this study would benefit from the use of additional models. We were unable to generate *Sox10* knockout clones in an additional mouse melanoma cell line, B16F10, and speculate that this cell line may rely strongly on SOX10 for proliferation. Lastly, we were limited in our study of CEACAM1 due to the complex regulation of its expression by alternative splicing, its interaction with various binding partners, and post-translational modification. Further analysis of the role of CEACAM1 alternative splicing and post-translational modification in modulating tumor growth is an interesting avenue for future studies. Overall, our data demonstrate that SOX10 regulates anti-tumor immunity, providing further insight into the complex role of SOX10 in melanoma and expanding our understanding of how it may regulate melanoma tumor growth.

STAR⋆METHODS

RESOURCE AVAILABILITY

Lead contact—Further information and requests for resources and reagents should be directed to and will be fulfilled by the lead contact, Andrew Aplin (Andrew.Aplin@jefferson.edu).

Materials availability—All novel reagents generated in this study are available from the lead contact and are typically dependent on drawing up of a Uniform Biological Materials Transfer Agreement (MTA) by the Technology Transfer Office at Thomas Jefferson University.

Data and code availability

- YUMM1.1 RNA-seq data generated in this study have been deposited in the NCBI BioProject database (BioProject: PRJNA688784) and are publicly available as of the date of publication. RNA-seq data from SOX10 knockout in MeWo cells are publicly available in BioProject (BioProject: PRJNA701949). ATAC-Seq data is available in the GEO database under the accession number GSE114557. TCGA data are publicly available from cbioportal.org. Single cell RNA-seq data used in this study are publicly available from the single cell portal (https://singlecell.broadinstitute.org/single_cell). All other raw data reported in this paper are available from the lead contact upon request.
- This paper does not report original code.
- Any additional information required to reanalyze the data reported in this paper is available from the lead contact upon request.

EXPERIMENTAL MODEL AND SUBJECT DETAILS

Cell culture—MeWo cells (donated by Dr. Barbara Bedogni, Case Western Reserve, Cleveland, OH in 2014), and B16F0 (purchased from ATCC, Manassas, VA) were cultured in DMEM with 10% fetal bovine serum (FBS). SKMel30 (donated by Dr. David Solit, Memorial Sloan Kettering Cancer Center, New York, NY) were cultured in RPMI-1640.

SKMel28 (purchased from ATCC) were cultured in MCDB 153 medium containing 20% Leibovitz L-15 medium, 2% FBS and 0.2% sodium bicarbonate (WM medium). YUMM1.1 (donated by Dr. Marcus Bosenberg, Yale School of Medicine, New Haven, CT in 2014) were cultured in DMEM/F12 with 10% FBS and 1% non-essential amino acids. 1014 cells (donated by Dr. Lionel Larue, Institut Curie, Orsay, France in 2017) were cultured in Ham's F-12 with 10% FBS and 1% penicillin/streptomycin. All cells were maintained at 37°C in 5% CO_2. Human cell lines were authenticated by sequencing at NRAS and BRAF loci and by STR analysis.

Animals—Six-eight weeks old male C57BL/6 mice were purchased from Jackson Laboratories. Male C57BL/6 mice were used for YUMM1.1 studies because this melanoma cell line was originally derived from male mice, which could generate an immune reaction when injected into immunocompetent female mice. Female C57BL/6 mice were used for 1014 studies because this melanoma cell line was originally derived from female mice. Male and female NOD.Cg-PrkdcscidIl2rgtm1Wjl/SzJ (NSG) mice and C57BL/6-Tg(TcraTcrb) 1100Mjb/J (OT-1) mice were originally purchased from Jackson Laboratories and bred at Thomas Jefferson University. Animals were randomly assigned to experimental groups, or evenly distributed between sexes for NSG experiments. B6.129S7-*Rag1*^{tm1Mom}/J (*Rag1* KO) mice were kindly provided by Dr. Luis Sigal, originally purchased from Jackson and bred at Thomas Jefferson University. All animal experiments were approved by the IACUC (protocol #1052) and performed in a facility at Thomas Jefferson University accredited by the Association for the Assessment and Accreditation of Laboratory Animal Care (AAALAC).

METHOD DETAILS

***In vivo* studies—**Cells were injected intradermally onto the backs of C57BL/6, NOD.*Cg-Prkdc*^{scid}*Il2rg*^{tm1Wjl}*/SzJ* (NSG), or B6. 129S7-*Rag1*^{tm1Mom}/J (*Rag1* KO) mice. Cell numbers were based on previous publications and past experiments (YUMM1.1 = 1×10^6 cells; 1014 = 5×10^5 cells) (Meeth et al., 2016). Tumors were considered fully formed when they reached ~50mm^3. For CD8+ depletion, animals were treated with 300 μg of anti-CD8α (clone 53–6.72) or the corresponding isotype control (Rat IgG2a, clone 2A3) (BioXCell; West Lebanon, NH) by intraperitoneal injection 2 days prior to tumor implantation and 2 times per week for the duration of the experiment. Treatments were determined based on previous publications. Animals were sacrificed when tumors exceeded 650mm^3 (Erkes et al., 2020).

Inhibitors, growth factors, and reagents—Recombinant IFN_γ was purchased from R&D Systems (Minneapolis, MN) and was used at a concentration of 100ng/mL for 48 hours.

CRISPR/Cas9—CRISPR/Cas9 gene editing was accomplished utilizing tools and protocols purchased from Dharmacon (Lafayette, CO). Briefly, a synthetic guide RNA transfection complex was prepared with 2 μL of 10 μM crRNA, 2 μL of 10 μM tracrRNA and 6 μL of Tris buffer. In a 24-well plate, cells were transfected for 48 hours with 10 μL of the RNA transfection complex, 0.2ng Cas9 plasmid, and 6 μg/well DharmaFECT Duo in

500 μL antibiotic-free media. Cells were then selected with puromycin for an additional 48 hours. Individual clones were picked and screened for efficient knockout. crRNA target sequences used were: SOX10 #1- TCTGGGTTCCCATCTGAC AT; CEACAM1 #1- GTAGACTCCCATATCCTTCA.

siRNA transfection—Cells were transfected for 4 hours with chemically synthesized siRNA at a final concentration of 25nmol/L using Lipofectamine RNAiMAX (Invitrogen) transfection reagent. Cells were harvested after 72 hours of knockdown. Target sequences used were as follows: non-targeting control (UGGUUUACAUGUCGACUAA), SOX10 #1 (GAACGAAAGUGACAAGCGC), SOX10 #2 (GAGAUCAGCC ACGAGGUAA), SOX10 #3 (GCGGGAAGCCUCACAUCGA). siRNAs were purchased from Dharmacon.

Lentiviral construction and transduction—Mouse HVEM was amplified from a *Tnfrsf14* (NM_178931.2) expression plasmid (Sino Biological; Chesterbrook, PA), cloned into pENTR/D-TOPO (Invitrogen; Carlsbad, CA), and LR recombined into pLenti-4/TO/V5-DEST. Mouse SOX10 was amplified from cDNA, cloned into pENTR/D-TOPO and LR recombined into pLentihygro/TO/V5-DEST. pDONR221-SOX10 was a gift from William Pavan, Addgene plasmid # 24749 (Cronin et al., 2009), and this was LR recombined into pLentipuro3/TO/GW/DEST for expression of human SOX10. Corresponding GFP control plasmids were pLentihygro/TO/GFP and pLentiPuro3/TO/GW/emGFP. Expression constructs and packaging plasmids pLP1, pLP2, pLP/VSVG were cotransfected into HEK293FT cells to generate viral particles. Cells were transduced with particles for 48 hours and then selected with zeocin, hygromycin, or puromycin, as previously described (Abel and Aplin, 2010).

Flow cytometry—Cells were stained for 30 mins with fluorochrome-conjugated antibodies: anti-mouse CEACAM1 (BioLegend; San Diego, CA; clone mAb-CC1), anti-mouse HVEM (BioLegend, clone HMHV-1B18), anti-mouse CD47 (BioLegend, clone miap301), anti-mouse PD-L1 (BioLegend, clone 10F.9G2), anti-mouse Galectin-9 (BioLegend, clone RG9–35), anti-human HVEM (BioLegend, clone 122), anti-human CEACAM1 (R&D Systems, clone 283340), anti-human CD47 (BioLegend, clone CC2C6), Armenian hamster IgG isotype control (BioLegend, clone HTK888), mouse IgG1 κ isotype control (BioLegend, clone MOPC-21), mouse IgG2b κ isotype control (BioLegend, clone MPC-11). Cells were fixed using the BD Cytofix/Cytoperm Kit from BD Biosciences (Franklin Lakes, NJ). For TIL analysis of mouse tumors, tumor pieces were minced with the gentleMACS™ Octo Dissociator using C Tubes (Miltenyi Biotec; Bergisch Gladback, Germany) in digestion media (1x HBSS, 0.1mg/ml Collagenase IA, 60 U/ml DNase I) and incubated at 37°C for 30 minutes with continuous rotation. Cells were washed with medium (RPMI 1640 with L-glutamine, 10% FBS, 1% PenStrep, and 5×10^{-5} β-mercaptoethanol), filtered through a 70μm nylon filter, fixed in formalin/BSA/PBS, and then incubated with Zombie Fixable Viability Dye (Bio-Legend) for 10 mins. After live/dead stain, cells were stained for 30 mins with fluorochrome-conjugated antibodies. Mouse tumors were stained with a cocktail of antibodies against CD45.2 (BioLegend, clone 104), CD3 (BioLegend, clone 17A2), CD8α (BioLegend, clone 53.6.7), CD8b (BioLegend, clone YTS156.7.7). Cells were fixed using the BD Cytofix/Cytoperm Kit (BD Biosciences). All samples were

analyzed on an LSR II, BD Celesta, or Fortessa flow cytometer (BD Biosciences) using FlowJo software (TreeStar, Ashaland, OR).

Western blot analysis—Protein lysates were prepared in Laemmli sample buffer, separated by SDS-PAGE, and proteins transferred to PVDF membranes. Immunoreactivity was detected using horseradish peroxidase-conjugated secondary antibodies (CalBioTech; Spring Valley, CA) and chemiluminescence substrate (ThermoScientific; Waltham, MA) on a Versadoc Imaging System (Bio-Rad; Hercules, CA). For detection of human SOX10 (#D5V9L) and CD47 (#D3O7P), mouse MITF (#D5G7V), mouse ZEB1 (#E2G6Y), or human and mouse CEACAM1 (#D1P4T) antibodies were purchased from Cell Signaling Technology (Danver, MA). Mouse CEACAM1 polyclonal antibody (#AF6480) was purchased from R&D Systems. ACTIN (A2066) antibody was purchased from Sigma (St. Louis, MO). Mouse SOX10 antibody (Clone A-2) was purchased from Santa Cruz (Dallas, TX). TYROSINASE (ab61294), GP100 (ab137078), and MELAN-A (ab210546) antibodies were purchased from Abcam (Cambridge, United Kingdom).

IncuCyte® live cell analysis—Cells were trypsinized and plated onto a 6-well plate. Photomicrographs were taken every 2 hours using an Incucyte Live cell imager (Essen Biosciences; Ann Arbor, MI). Plate confluence was measured using IncuCyte® software and presented as percentages.

QUANTIFICATION AND STATISTICAL ANALYSIS

Statistics—For *in* vivo studies, survival curves and curves showing % tumor-free mice were analyzed using a Log-rank (Mantel-Cox) test. A p value of < 0.05 was considered statistically significant. Significance is denoted by $*p < 0.05$, $**p < 0.01$, $***p < 0.001$. For analysis of single cell RNA-seq data, zero-inflated negative binomial (ZINB) regression models were used to model single cell RNA-seq counts of TNFRSF14 (HVEM) and CEACAM1 as dependent on SOX10 counts and the total RNA-seq counts per cell as an exposure. The ZINB regression model includes a mean model for the negative binomial mean of TNFRSF14/CEACAM1 count as dependent on SOX10 counts, and a zero-inflation probability model, which is essentially a logistic regression predicting the odds of zero counts as dependent on SOX10 counts.

RNA-sequencing analysis—RNA-seq libraries were prepared from triplicate samples of parental YUMM1.1 and *Sox10* KO clones (#1.41 and #1.51) using RNeasy plant mini kit (QIAGEN; Hilden, Germany) following manufacturer's protocol. The final libraries at the concentration of 4nM were sequenced on NextSeq 500 using 75bp paired-end chemistry. Raw FASTQ sequencing reads were mapped against the reference genome of *Mus musculus* Ensembl Version GRCm38 utilizing further information from the gene transfer format (.gtf) annotation from GENCODE version M19 using RSEM (Li and Dewey, 2011). Total read counts, and normalized Transcripts Per Million (TPM) were obtained using RSEM's calculate-expression function. Before differential expression, batch effects or sample heterogeneity was tested using iSeqQC (Kumar et al., 2020). Differential gene expression was performed between *Sox10* KO clones (#1.41 and #1.51) versus parental control using the DESeq2 package in R/Bioconductor (Love et al., 2014). Genes were

considered differentially expressed (DE) if they had adjusted p value % 0.05 and absolute fold change ≥ 2. All plots were constructed using R/Bioconductor. Gene Set Enrichment Analysis (GSEA) was performed to evaluate Kyoto Encyclopedia of Genes and Genomes (KEGG) terms in the resulting differential expression lists. The DESeq2 test statistic was used as a ranking metric to perform GSEA in pre-ranked mode, with genes having zero base mean or "NA" test statistic values filtered out to avoid providing numerous duplicate values to GSEA. GSEA pre-ranked analysis was performed using the "weighted" enrichment statistic (Subramanian et al., 2005).

TCGA analyses—The Cancer Genome Atlas (TCGA) SKCM RNA sequencing (RNA-seq) V2 RSEM normalized counts data were retrieved from http://www.cbioportal.org/ (Cerami et al., 2012; Gao et al., 2013), and analyzed for gene set enrichment using IGV_2.8.6 software. For all correlation analyses, TCGA Firehose Legacy Skin Cutaneous melanoma dataset was utilized; for pan-cancer analyses, TCGA Pan-Cancer Atlas Skin Cutaneous melanoma dataset was utilized. For analysis of lymphocyte levels in TCGA samples, each sample was previously classified by Lscore, which is equal to the sum of lymphocyte distribution and lymphocyte density scores as determined by sample histology (Cancer Genome Atlas Network, 2015). For patients with multiple samples, only metastatic samples were retained, and mRNA expression from the Broad GDAC Firehose data run (stddata__2016_01_28) were correlated with Lscore.

ATAC-Seq analysis—ATAC Seq. merged peaks raw counts data for SOX10 time-series knockdown and control samples from two melanoma cell lines were obtained from the Gene Expression Omnibus (GEO) under the accession number GSE114557. DESeq2 (v 1.28.1) (Love et al., 2014) was used to perform differential peak analysis. Analysis was performed between SOX10 KD and control samples, while controlling for cell line.

Supplementary Material

Refer to Web version on PubMed Central for supplementary material.

ACKNOWLEDGMENTS

This work is supported by grants from National Institutes of Health (NIH)/National Cancer Institute (NCI) R01s CA182635 and CA160495 to A.E.A., F99 CA245552 to S.R.R. S.R.R. was also supported by T32 GM100836 (PI: Dr. Jeffrey Benovic). Additionally, the study was supported by Dr. Miriam and Sheldon G. Adelson Medical Research Foundation awards to A.E.A. The Sidney Kimmel Cancer Center Flow Cytometry, Translational Pathology and Meta-Omics core facilities are supported by NIH/NCI Cancer Center Support Grant (P30 CA056036). We are grateful to Dr. Meenhard Herlyn (The Wistar Institute), Dr. Marcus Bosenberg (Yale School of Medicine), Dr. Barbara Bedogni (Case Western Reserve), and Dr. David Solit (Memorial Sloan Kettering Cancer Center) for generously providing cell lines; to Dr. Luis Sigal for providing B6. 129S7-*Rag1*^{tm1Mom}/J (*Rag1* KO) mice; and to Nicole Wilski for advising on flow cytometry experiments.

REFERENCES

Abel EV, and Aplin AE (2010). FOXD3 is a mutant B-RAF-regulated inhibitor of G(1)-S progression in melanoma cells. Cancer Res 70, 2891–2900. [PubMed: 20332228]

Ashkenazi S, Ortenberg R, Besser M, Schachter J, and Markel G (2016). SOX9 indirectly regulates CEACAM1 expression and immune resistance in melanoma cells. Oncotarget 7, 30166–30177. [PubMed: 26885752]

Atefi M, Avramis E, Lassen A, Wong DJL, Robert L, Foulad D, Cerniglia M, Titz B, Chodon T, Graeber TG, et al. (2014). Effects of MAPK and PI3K pathways on PD-L1 expression in melanoma. Clin. Cancer Res 20, 3446–3457. [PubMed: 24812408]

Bravo González-Blas C, Minnoye L, Papasokrati D, Aibar S, Hulselmans G, Christiaens V, Davie K, Wouters J, and Aerts S (2019). cisTopic: cis-regulatory topic modeling on single-cell ATAC-seq data. Nat. Methods 16, 397–400. [PubMed: 30962623]

Cai G, Anumanthan A, Brown JA, Greenfield EA, Zhu B, and Freeman GJ (2008). CD160 inhibits activation of human CD4+ T cells through interaction with herpesvirus entry mediator. Nat. Immunol 9, 176–185. [PubMed: 18193050]

Cancer Genome Atlas Network (2015). Genomic classification of cutaneous melanoma. Cell 161, 1681–1696. [PubMed: 26091043]

Cerami E, Gao J, Dogrusoz U, Gross BE, Sumer SO, Aksoy BA, Jacobsen A, Byrne CJ, Heuer ML, Larsson E, et al. (2012). The cBio cancer genomics portal: an open platform for exploring multidimensional cancer genomics data. Cancer Discov 2, 401–404. [PubMed: 22588877]

Chen D, Iijima H, Nagaishi T, Nakajima A, Russell S, Raychowdhury R, Morales V, Rudd CE, Utku N, and Blumberg RS (2004). Carcinoembryonic antigen-related cellular adhesion molecule 1 isoforms alternatively inhibit and costimulate human T cell function. J. Immunol 172, 3535–3543. [PubMed: 15004154]

Chen Z, Chen L, Baker K, Olszak T, Zeissig S, Huang Y-H, Kuo TT, Mandelboim O, Beauchemin N, Lanier LL, and Blumberg RS (2011). CEACAM1 dampens antitumor immunity by down-regulating NKG2D ligand expression on tumor cells. J. Exp. Med 208,2633–2640. [PubMed: 22143889]

Chew G-L, Campbell AE, DeNeef E, Sutliff NA, Shadle SC, Tapscott SJ, and Bradley RK (2019). DUX4 suppresses MHC class I to promote cancer immune evasion and resistance to checkpoint blockade. Dev. Cell 50, 658–671.e7. [PubMed: 31327741]

Cronin JC, Wunderlich J, Loftus SK, Prickett TD, Wei X, Ridd K, Vemula S, Burrell AS, Agrawal NS, Lin JC, et al. (2009). Frequent mutations inthe MITF pathway in melanoma. Pigment Cell Melanoma Res 22, 435–444. [PubMed: 19422606]

Cronin JC, Watkins-Chow DE, Incao A, Hasskamp JH, Schönewolf N, Aoude LG, Hayward NK, Bastian BC, Dummer R, Loftus SK, and Pavan WJ (2013). SOX10 ablation arrests cell cycle, induces senescence, and suppresses melanomagenesis. Cancer Res 73, 5709–5718. [PubMed: 23913827]

Dankner M, Gray-Owen SD, Huang Y-H, Blumberg RS, and Beauchemin N (2017). CEACAM1 as a multi-purpose target for cancer immunotherapy. OncoImmunology 6, e1328336. [PubMed: 28811966]

Erkes DA, Cai W, Sanchez IM, Purwin TJ, Rogers C, Field CO, Berger AC, Hartsough EJ, Rodeck U, Alnemri ES, and Aplin AE (2020). Mutant BRAF and MEK inhibitors regulate the tumor immune microen-vironment via pyroptosis. Cancer Discov 10, 254–269. [PubMed: 31796433]

Fufa TD, Harris ML, Watkins-Chow DE, Levy D, Gorkin DU, Gildea DE, Song L, Safi A, Crawford GE, Sviderskaya EV, et al. (2015). Genomic analysis reveals distinct mechanisms and functional classes of SOX10-regulated genes in melanocytes. Hum. Mol. Genet 24, 5433–5450. [PubMed: 26206884]

Gao J, Aksoy BA, Dogrusoz U, Dresdner G, Gross B, Sumer SO, Sun Y, Jacobsen A, Sinha R, Larsson E, et al. (2013). Integrative analysis of complex cancer genomics and clinical profiles using the cBioPortal. Sci. Signal 6, pl1. [PubMed: 23550210]

Garcia-Diaz A, Shin DS, Moreno BH, Saco J, Escuin-Ordinas H, Rodriguez GA, Zaretsky JM, Sun L, Hugo W, Wang X, et al. (2017). Interferon receptor signaling pathways regulating PD-L1 and PD-L2 expression. Cell Rep 19, 1189–1201. [PubMed: 28494868]

Gray-Owen SD, and Blumberg RS (2006). CEACAM1: contact-dependent control of immunity. Nat. Rev. Immunol 6, 433–446. [PubMed: 16724098]

Houde C, Roy S, Leung N, Nicholson DW, and Beauchemin N (2003). The cell adhesion molecule CEACAM1-L is a substrate of caspase-3-mediated cleavage in apoptotic mouse intestinal cells. J. Biol. Chem 278, 16929–16935. [PubMed: 12637508]

Huang Y-H, Zhu C, Kondo Y, Anderson AC, Gandhi A, Russell A, Dougan SK, Petersen B-S, Melum E, Pertel T, et al. (2015). CEACAM1 regulates TIM-3-mediated tolerance and exhaustion. Nature 517, 386–390. [PubMed: 25363763]

Huntington ND, Cursons J, and Rautela J (2020). The cancer-natural killer cell immunity cycle. Nat. Rev. Cancer 20, 437–454. [PubMed: 32581320]

Inoue T, Sho M, Yasuda S, Nishiwada S, Nakamura S, Ueda T, Nishigori N, Kawasaki K, Obara S, Nakamoto T, et al. (2015). HVEM expression contributes to tumor progression and prognosis in human colorectal cancer. Anti cancer Res 35, 1361–1367.

Jerby-Arnon L, Shah P, Cuoco MS, Rodman C, Su M-J, Melms JC, Leeson R, Kanodia A, Mei S, Lin J-R, et al. (2018). A cancer cell program promotes T cell exclusion and resistance to checkpoint blockade. Cell 175, 984–997.e24. [PubMed: 30388455]

Kanellopoulos-Langevin C, Caucheteux SM, Verbeke P, and Ojcius DM (2003). Tolerance of the fetus by the maternal immune system: role of inflammatory mediators at the feto-maternal interface. Reprod. Biol. Endocrinol 1, 121. [PubMed: 14651750]

Kudo-Saito C, Shirako H, Takeuchi T, and Kawakami Y (2009). Cancer metastasis is accelerated through immunosuppression during Snail-induced EMT of cancer cells. Cancer Cell 15, 195–206. [PubMed: 19249678]

Kumar G, Ertel A, Feldman G, Kupper J, and Fortina P (2020). iSeqQC: a tool for expression-based quality control in RNA sequencing. BMC Bioinformatics 21, 56. [PubMed: 32054449]

Lan X, Li S, Gao H, Nanding A, Quan L, Yang C, Ding S, and Xue Y (2017). Increased BTLA and HVEM in gastric cancer are associated with progression and poor prognosis. OncoTargets Ther 10, 919–926.

Largeot A, Pagano G, Gonder S, Moussay E, and Paggetti J (2019). The B-side of cancer immunity: the underrated tune. Cells 8, 449.

Li B, and Dewey CN (2011). RSEM: accurate transcript quantification from RNA-Seq data with or without a reference genome. BMC Bioinformatics 12, 323. [PubMed: 21816040]

Love MI, Huber W, and Anders S (2014). Moderated estimation of fold change and dispersion for RNA-seq data with DESeq2. Genome Biol 15, 550. [PubMed: 25516281]

Malissen N, Macagno N, Granjeaud S, Granier C, Moutardier V, Gaudy-Marqueste C, Habel N, Mandavit M, Guillot B, Pasero C, et al. (2019). HVEM has a broader expression than PD-L1 and constitutes a negative prognostic marker and potential treatment target for melanoma. OncoImmunology 8, e1665976. [PubMed: 31741766]

Markel G, Lieberman N, Katz G, Arnon TI, Lotem M, Drize O, Blumberg RS, Bar-Haim E, Mader R, Eisenbach L, and Mandelboim O (2002). CD66a interactions between human melanoma and NK cells: a novel class I MHC-independent inhibitory mechanism of cytotoxicity. J. Immunol 168, 2803–2810. [PubMed: 11884449]

Markel G, Seidman R, Cohen Y, Besser MJ, Sinai TC, Treves AJ, Orenstein A, Berger R, and Schachter J (2009). Dynamic expression of protective CEACAM1 on melanoma cells during specific immune attack. Immunology 126, 186–200. [PubMed: 18557789]

Meeth K, Wang JX, Micevic G, Damsky W, and Bosenberg MW (2016). The YUMM lines: a series of congenic mouse melanoma cell lines with defined genetic alterations. Pigment Cell Melanoma Res 29, 590–597. [PubMed: 27287723]

Miko E, Meggyes M, Doba K, Barakonyi A, and Szereday L (2019). Immune checkpoint molecules in reproductive immunology. Front. Immunol 10, 846. [PubMed: 31057559]

Mintz MA, Felce JH, Chou MY, Mayya V, Xu Y, Shui J-W, An J, Li Z, Marson A, Okada T, et al. (2019). The HVEM-BTLA axis restrains T cell help to germinal center B cells and functions as a cell-extrinsic suppressor in lymphomagenesis. Immunity 51, 310–323.e7. [PubMed: 31204070]

Mortarini R, Scarito A, Nonaka D, Zanon M, Bersani I, Montaldi E, Pennacchioli E, Patuzzo R, Santinami M, and Anichini A (2005). Constitutive expression and costimulatory function of LIGHT/TNFSF14 on human melanoma cells and melanoma-derived microvesicles. Cancer Res 65, 3428–3436. [PubMed: 15833878]

Murphy KM, Nelson CA, and Sedý JR (2006). Balancing co-stimulation and inhibition with BTLA and HVEM. Nat. Rev. Immunol 6, 671–681. [PubMed: 16932752]

Pathria P, Louis TL, and Varner JA (2019). Targeting tumor-associated macrophages in cancer. Trends Immunol 40, 310–327. [PubMed: 30890304]

Pérez-Guijarro E, Yang HH, Araya RE, El Meskini R, Michael HT, Vodnala SK, Marie KL, Smith C, Chin S, Lam KC, et al. (2020). Multimodel preclinical platform predicts clinical response of melanoma to immunotherapy. Nat. Med 26, 781–791. [PubMed: 32284588]

Petit V, Raymond J, Alberti C, Pouteaux M, Gallagher SJ, Nguyen MQ, Aplin AE, Delmas V, and Larue L (2019). C57BL/6 congenic mouse NRASQ61K melanoma cell lines are highly sensitive to the combination of Mek and Akt inhibitors in vitro and in vivo. Pigment Cell Melanoma Res 32, 829–841. [PubMed: 31251472]

Rambow F, Rogiers A, Marin-Bejar O, Aibar S, Femel J, Dewaele M, Karras P, Brown D, Chang YH, Debiec-Rychter M, et al. (2018). Toward minimal residual disease-directed therapy in melanoma. Cell 174, 843–855.e19. [PubMed: 30017245]

Rambow F, Marine JC, and Goding CR (2019). Melanoma plasticity and phenotypic diversity: therapeutic barriers and opportunities. Genes Dev 33, 1295–1318. [PubMed: 31575676]

Rodriguez-Barbosa JI, Schneider P, Weigert A, Lee K-M, Kim T-J, Perez-Simon J-A, and Del Rio M-L (2019). HVEM, a cosignaling molecular switch, and its interactions with BTLA, CD160 and LIGHT. Cell. Mol. Immunol 16, 679–682. [PubMed: 31160757]

Rosenbaum SR, Knecht M, Mollaee M, Zhong Z, Erkes DA, McCue PA, Chervoneva I, Berger AC, Lo JA, Fisher DE, et al. (2020). FOXD3 regulates VISTA expression in melanoma. Cell Rep 30, 510–524.e6. [PubMed: 31940493]

Sedy JR, Gavrieli M, Potter KG, Hurchla MA, Lindsley RC, Hildner K, Scheu S, Pfeffer K, Ware CF, Murphy TL, and Murphy KM (2005). B and T lymphocyte attenuator regulates T cell activation through interaction with herpesvirus entry mediator. Nat. Immunol 6, 90–98. [PubMed: 15568026]

Shakhova O, Zingg D, Schaefer SM, Hari L, Civenni G, Blunschi J, Claudinot S, Okoniewski M, Beermann F, Mihic-Probst D, et al. (2012). Sox10 promotes the formation and maintenance of giant congenital naevi and melanoma. Nat. Cell Biol 14, 882–890. [PubMed: 22772081]

Sienel W, Dango S, Woelfle U, Morresi-Hauf A, Wagener C, Brümmer J, Mutschler W, Passlick B, and Pantel K (2003). Elevated expression of carcinoembryonic antigen-related cell adhesion molecule 1 promotes progression of non-small cell lung cancer. Clin. Cancer Res 9, 2260–2266. [PubMed: 12796394]

Subramanian A, Tamayo P, Mootha VK, Mukherjee S, Ebert BL, Gillette MA, Paulovich A, Pomeroy SL, Golub TR, Lander ES, and Mesirov JP (2005). Gene set enrichment analysis: a knowledge-based approach for interpreting genome-wide expression profiles. Proc. Natl. Acad. Sci. USA 102, 15545–15550. [PubMed: 16199517]

Sun C, Wang L, Huang S, Heynen GJJE, Prahallad A, Robert C, Haanen J, Blank C, Wesseling J, Willems SM, et al. (2014). Reversible and adaptive resistance to BRAF(V600E) inhibition in melanoma. Nature 508, 118–122. [PubMed: 24670642]

Takeuchi A, Yokoyama S, Nakamori M, Nakamura M, Ojima T, Yamaguchi S, Mitani Y, Shively JE, and Yamaue H (2019). Loss of CEACAM1 is associated with poor prognosis and peritoneal dissemination of patients with gastric cancer. Sci. Rep 9, 12702. [PubMed: 31481751]

Tamada K, Shimozaki K, Chapoval AI, Zhu G, Sica G, Flies D, Boone T, Hsu H, Fu Y-X, Nagata S, et al. (2000). Modulation of T-cell-mediated immunity in tumor and graft-versus-host disease models through the LIGHT co-stimulatory pathway. Nat. Med 6, 283–289. [PubMed: 10700230]

Tang M, Cao X, Li Y, Li G-Q, He Q-H, Li S-J, Chen J, Xu G-L, and Zhang K-Q (2019). High expression of herpes virus entry mediator is associated with poor prognosis in clear cell renal cell carcinoma. Am. J. Cancer Res 9, 975–987. [PubMed: 31218105]

Tersigni C, Meli F, Neri C, Iacoangeli A, Franco R, Lanzone A, Scambia G, and Di Simone N (2020). Role of human leukocyte antigens at the feto-maternal interface in normal and pathological pregnancy: an update. Int. J. Mol. Sci 21, 4756.

Thiem A, Hesbacher S, Kneitz H, di Primio T, Heppt MV, Hermanns HM, Goebeler M, Meierjohann S, Houben R, and Schrama D (2019). IFN-gamma-induced PD-L1 expression in melanoma depends on p53 expression. J. Exp. Clin. Cancer Res 38, 397. [PubMed: 31506076]

Thies A, Moll I, Berger J, Wagener C, Brümmer J, Schulze H-J, Brunner G, and Schumacher U (2002). CEACAM1 expression in cutaneous malignant melanoma predicts the development of metastatic disease. J. Clin. Oncol 20, 2530–2536. [PubMed: 12011132]

Ullrich N, Heinemann A, Nilewski E, Scheffrahn I, Klode J, Scherag A, Schadendorf D, Singer BB, and Helfrich I (2015). CEACAM1–3S drives melanoma cells into NK cell-mediated cytolysis and enhances patient survival. Cancer Res 75, 1897–1907. [PubMed: 25744717]

Vartuli RL, Zhou H, Zhang L, Powers RK, Klarquist J, Rudra P, Vincent MY, Ghosh D, Costello JC, Kedl RM, et al. (2018). Eya3 promotes breast tumor-associated immune suppression via threonine phosphatase-mediated PD-L1 upregulation. J. Clin. Invest 128, 2535–2550. [PubMed: 29757193]

Verfaillie A, Imrichova H, Atak ZK, Dewaele M, Rambow F, Hulselmans G, Christiaens V, Svetlichnyy D, Luciani F, Van den Mooter L, et al. (2015). Decoding the regulatory landscape of melanoma reveals TEADS as regulators of the invasive cell state. Nat. Commun 6, 6683. [PubMed: 25865119]

Wicklein D, Otto B, Suling A, Elies E, Lüers G, Lange T, Feldhaus S, Maar H, Schröder-Schwarz J, Brunner G, et al. (2018). CEACAM1 promotes melanoma metastasis and is involved in the regulation of the EMT associated gene network in melanoma cells. Sci. Rep 8, 11893. [PubMed: 30089785]

Wouters J, Kalender-Atak Z, Minnoye L, Spanier KI, De Waegeneer M, Bravo González-Blas C, Mauduit D, Davie K, Hulselmans G, Najem A, et al. (2020). Robust gene expression programs underlie recurrent cell states and phenotype switching in melanoma. Nat. Cell Biol 22, 986–998. [PubMed: 32753671]

Zalzali H, Naudin C, Bastide P, Quittau-Prévostel C, Yaghi C, Poulat F, Jay P, and Blache P (2008). CEACAM1, a SOX9 direct transcriptional target identified in the colon epithelium. Oncogene 27, 7131–7138. [PubMed: 18794798]

Zhang T, Ye L, Han L, He Q, and Zhu J (2016). Knockdown of HVEM, a lymphocyte regulator gene, in ovarian cancer cells increases sensitivity to activated T cells. Oncol. Res 24, 189–196. [PubMed: 27458100]

Highlights

- *Sox10* knockout reduces expression of the immune checkpoint proteins HVEM and CEACAM1
- In immune-competent models, *Sox10* knockout reduces melanoma tumor growth
- *Sox10* effects on tumor growth are dependent, in part, on CD8+ T cells
- In TCGA cutaneous melanoma data, *Sox10* is inversely correlated with immune pathways

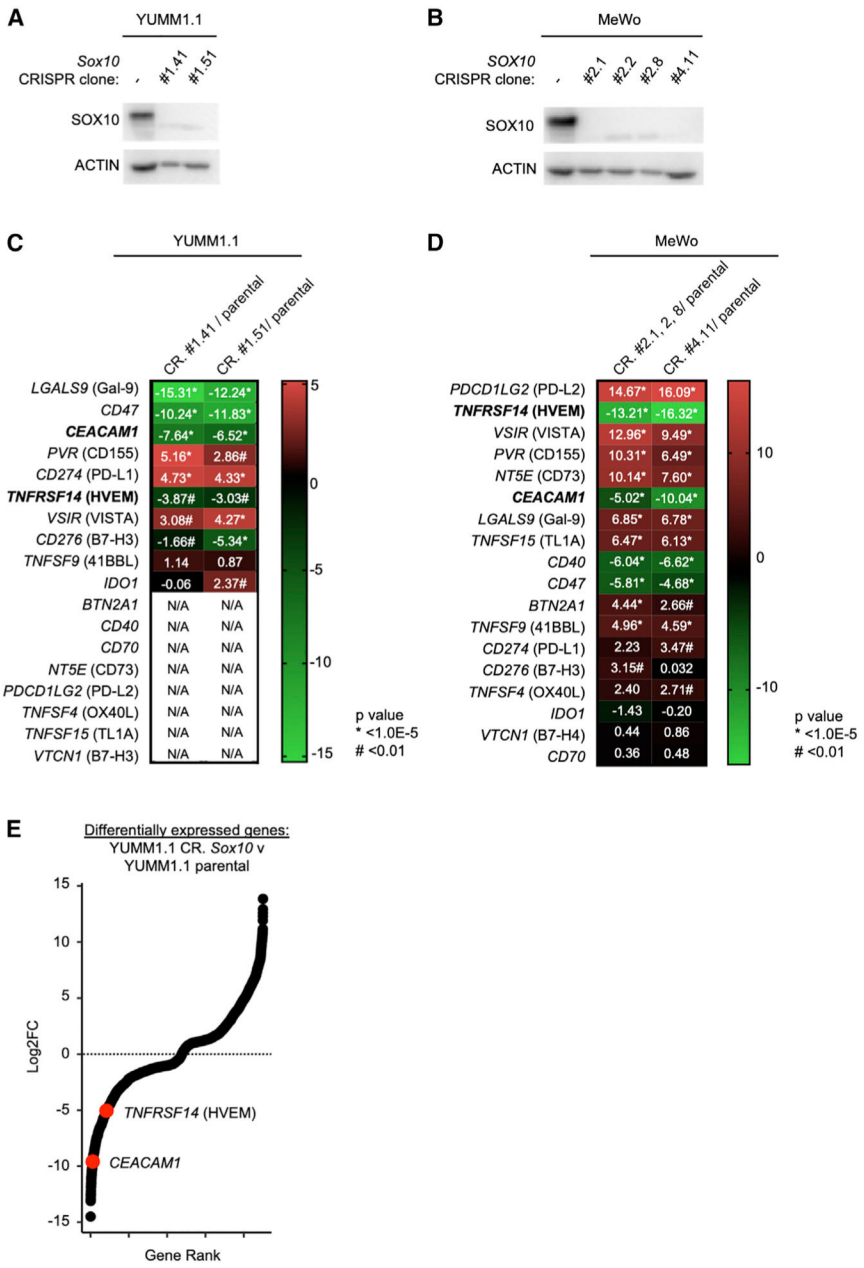

Figure 1. SOX10 alters mRNA levels of immune checkpoint proteins

(A) SOX10 expression was probed by western blot in parental mouse melanoma YUMM1.1 cells and *Sox10* knockout clones.

(B) SOX10 expression was probed by western blot in parental human melanoma MeWo cells and *SOX10* knockout clones.

(C) RNA was collected from 3 biological replicates of parental and *Sox10* knockout clones, RNA-seq was performed, and data were mined for immune checkpoint proteins. Shown are fold changes of mRNA levels in *Sox10* knockout clone #1.41 (CR. #1.41) or *Sox10* knockout clone #1.51 (CR. #1.51) versus parental. *p < 1.0E -5; #p < 0.01.

(D) RNA-seq was performed on parental and *SOX10* knockout clones, and data were mined for immune checkpoint proteins. Shown are fold changes of mRNA levels across *SOX10*

knockout clones #2.1, 2.2, and 2.8 versus parental (CR. #2.1, 2, and 8) or *SOX10* knockout clone #4.11 (CR. #4.11). *p < 1.0E -5; #p < 0.01.
(E) Differentially expressed genes in YUMM1.1 *Sox10* knockout cells compared to those in parental cells were plotted by gene rank against log2 fold change.

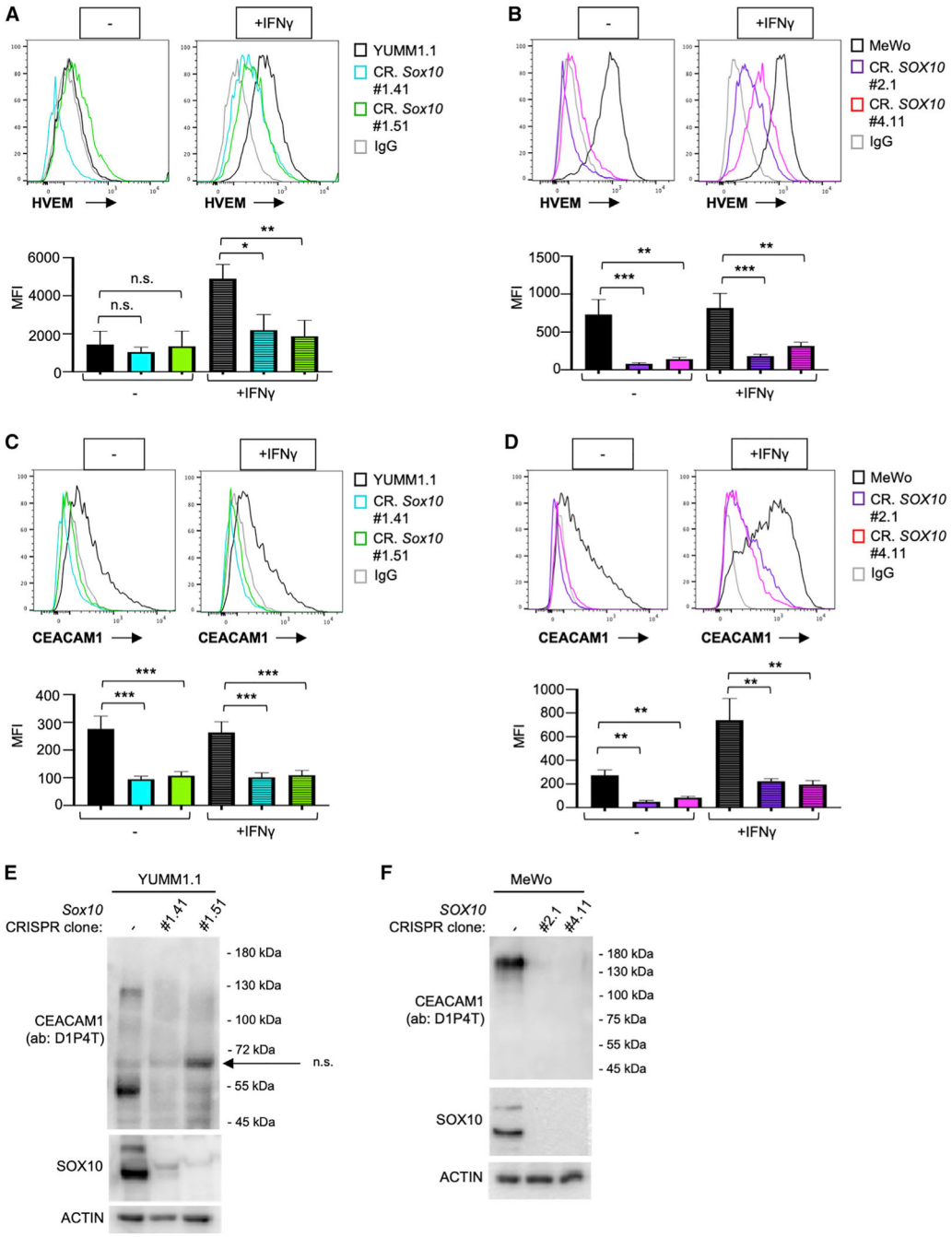

Figure 2. *SOX10* knockout reduces expression of HVEM and CEACAM1

(A) Parental mouse melanoma YUMM1.1 cells and *Sox10* knockout clones were treated with or without 100 ng/mL IFN$_\gamma$, and HVEM expression was probed by flow cytometry staining. Mean fluorescence intensity (MFI) was quantified.

(B) Parental human melanoma MeWo cells and *SOX10* knockout clones were treated with or without 100 ng/mL IFN$_\gamma$. HVEM expression was probed by flow cytometry staining, and MFI was quantified.

(C) Parental mouse melanoma YUMM1.1 cells and *Sox10* knockout clones were treated with or without 100 ng/mL IFN_{γ}. CEACAM1 expression was probed by flow cytometry staining, and MFI was quantified.

(D) Parental human melanoma MeWo cells and *SOX10* knockout clones were treated with or without 100 ng/mL IFN_{γ}. CEACAM1 expression was probed by flow cytometry staining, and MFI was quantified.

(E) CEACAM1 expression was probed by western blot in parental mouse melanoma YUMM1.1 cells and *Sox10* knockout clones. The arrow indicates a nonspecific band ("n.s.").

(F) CEACAM1 expression was probed by western blot in parental human melanoma MeWo cells and *SOX10* knockout clones. All data in this figure represent 3 biological replicates; *$p < 0.05$, **$p < 0.01$, ***$p < 0.001$.

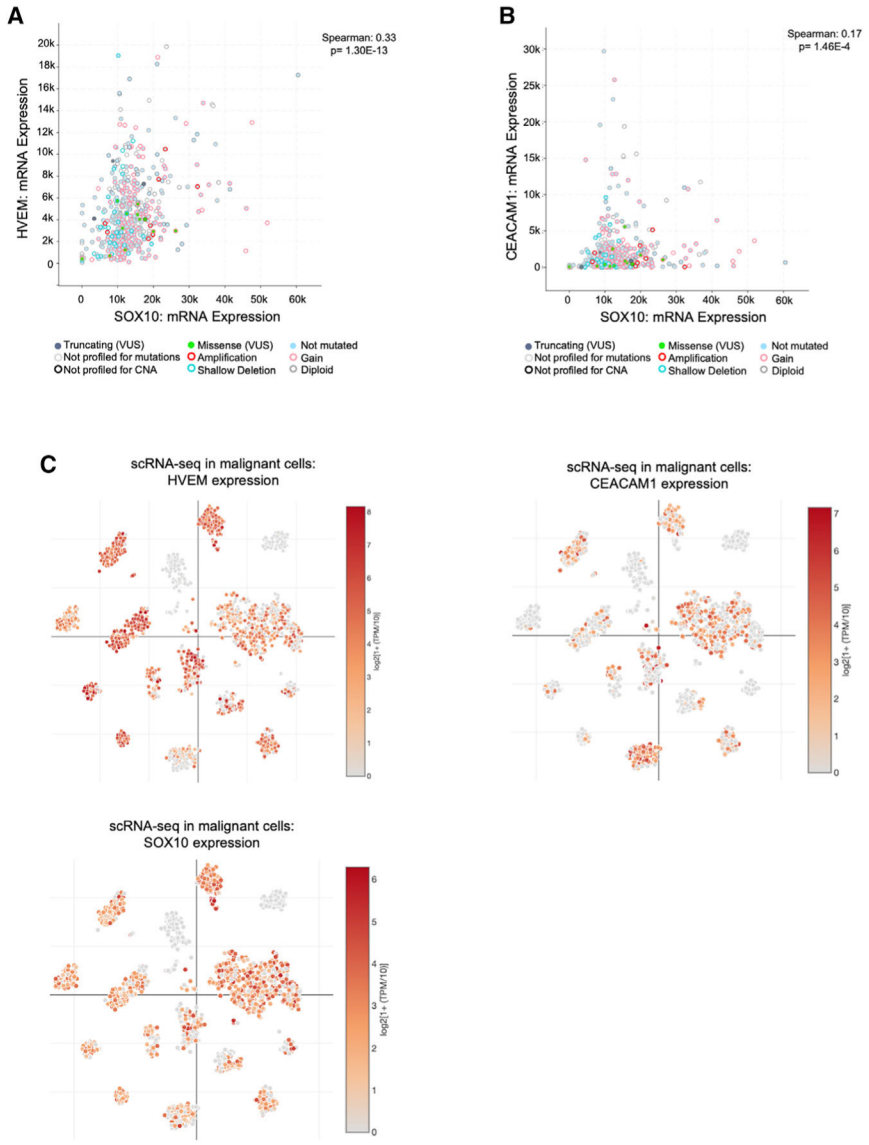

Figure 3. SOX10 is correlated with CEACAM1 and HVEM expression in patient datasets

(A) RNA-seq from the melanoma TCGA dataset was visualized using cBioportal, and the mRNA expression level of HVEM (*TNFRSF14*) was plotted versus SOX10 expression (Cerami et al., 2012; Gao et al., 2013). Shown are values batch normalized from Illumina HiSeq_RNASeqV2. SOX10 mutation type, structural variant, and copy number are indicated for each sample.

(B) RNA-seq from the melanoma TCGA dataset was visualized using cBioportal, and the mRNA expression level of CEACAM1 was plotted versus SOX10 express ion (Cerami et al., 2012; Gao et al., 2013). Shown are values batch normalized from Illumina HiSeq_RNASeqV2. SOX10 mutation type, structural variant, and copy number are indicated for each sample.

(C) Single-cell RNA-seq data of malignant cells (Jerby-Arnon et al., 2018) were visualized by t-distributed stochastic neighbor embedding (tSNE) plots by using the Single Cell portal

(https://singlecell.broadinstitute.org/single_cell), whereby each cluster represents a distinct melanoma tumor and each circle represents an individual cell.

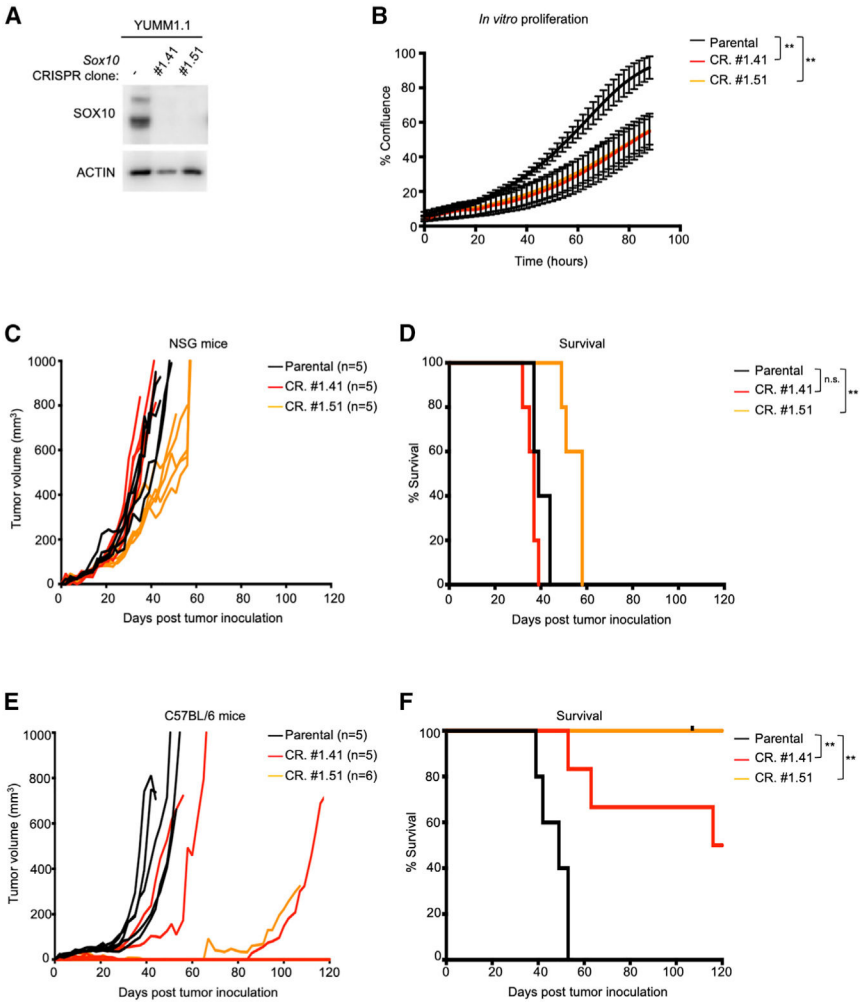

Figure 4. *Sox10* ablation reduces tumor growth, and this effect is exacerbated in an immune-competent setting

(A) CRISPR-Cas9 was used to knockout *Sox10* from the mouse melanoma cell line YUMM1.1. Cell lysates were probed by western blot, and *Sox10* knockout was verified in two individual clones.

(B) *In vitro* cell growth of *Sox10* knockout clones was evaluated using the IncuCyte live-cell imager. Data are representative of 3 independent experiments, each with 3 technical replicates.

(C) YUMM1.1 parental or *Sox10* knockout cells were injected into NSG mice. Tumors were measured using digital caliper every 2–3 days. Data were collected from 5 mice per group.

(D) Related to (C), mice were sacrificed when tumors exceeded 650 mm^3 in volume. Shown is a Kaplan-Meier survival curve.

(E) YUMM1.1 parental or *Sox10* knockout clones #1.41 or #1.51 were injected into C57BL/6 mice, and tumors were measured by caliper every 2–3 days. Data were collected from 5–6 mice per group.

(F) Related to (E), mice were sacrificed when tumors exceeded 650 mm^3 in volume. Shown is a Kaplan-Meier survival curve. **$p < 0.01$.

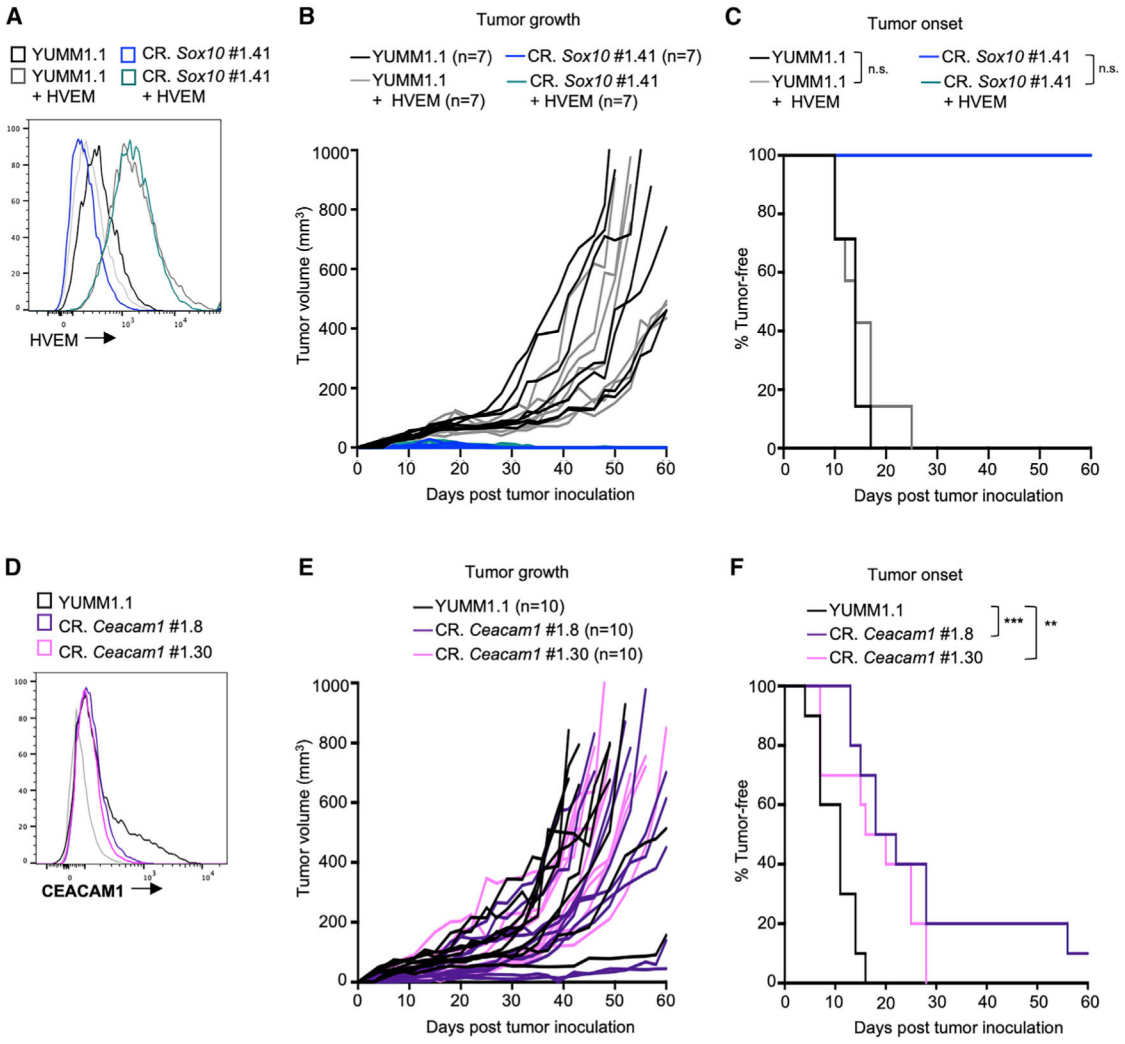

Figure 5. Effects of HVEM or CEACAM1 alone on tumor growth

(A) HVEM was expressed in YUMM1.1 parental and CR. #1.41 *Sox10* knockout cells by lentiviral transduction. HVEM expression was validated by flow cytometry staining. Data are representative of 3 biological replicates. An unstained control is shown in light gray.

(B) YUMM1.1 parental, CR. #1.41 *Sox10* knockout cells, or HVEM-overexpressing cells were injected into BL6 mice, and tumors were measured by digital caliper every 2–3 days. Data were collected from 7 mice per group.

(C) Related to (B), time-to-tumor onset was tracked. Tumors were considered fully formed when they reached ~50 mm^3.

(D) Two individual clones were generated from CRISPR-Cas9 knockout of *Ceacam1* in YUMM1.1 cells. CEACAM1 surface expression was evaluated by flow cytometry. Data are representative of 3 biological replicates. An unstained control is shown in light gray.

(E) YUMM1.1 parental, CR. #1.8, or CR. #1.30 *Ceacam1* knockout cells were injected into BL6 mice, and tumors were measured by caliper every 2–3 days. Data were collected from 10 mice per group.

(F) Related to (E), time-to-tumor onset was tracked. Tumors were considered fully formed when they reached ~50 mm^3.**p < 0.01, ***p < 0.001.

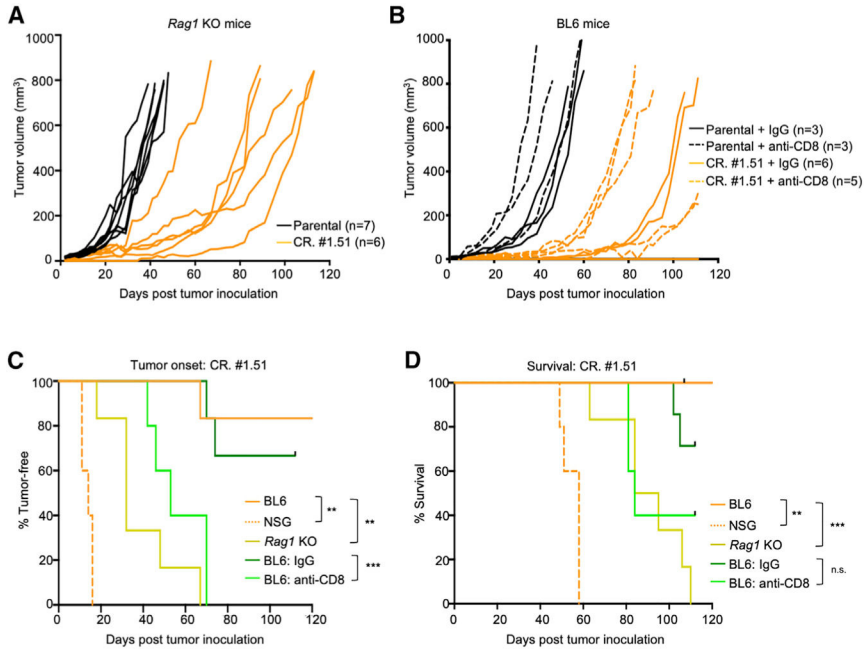

Figure 6. SOX10 effects on tumor growth are partially dependent on CD8+ T cells

(A) YUMM1.1 parental or *Sox10* knockout clone #1.51 cells were injected into *Rag1* knockout mice, and tumors were measured by caliper every 2–3 days. Data were collected from 6–7 mice per group.

(B) BL6 mice were treated with 300 μg of either CD8-depleting antibody or the relevant isotype control 2 days before tumor inoculation, and twice per week throughout the course of the experiment. YUMM1.1 parental (n = 3) or *Sox10* knockout clone #1.51 (n = 6) cells were injected into treated mice, and tumors were measured by caliper every 2–3 days.

(C) Related to (A), (B), and Figure 1C, and Figure 1E. Tumors were measured every 2–3 days by caliper measurement, and time-to-tumor onset was tracked. Tumors were considered fully formed when they reached 50 mm^3.

(D) Related to (C), mice were sacrificed when tumors exceeded 650 mm^3 in volume. Shown is a Kaplan-Meier survival curve. **p < 0.01, ***p < 0.001.

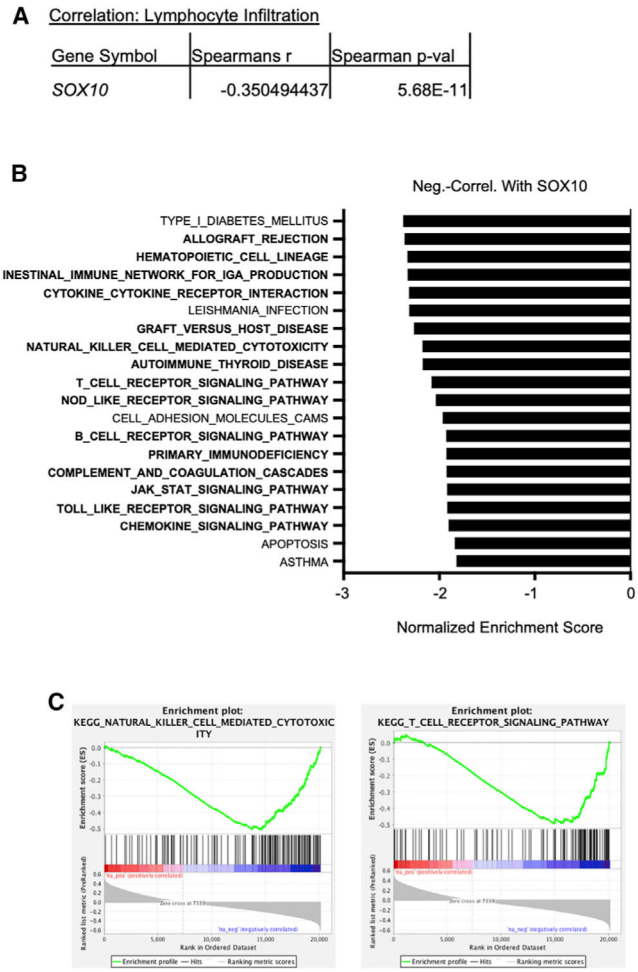

Figure 7. SOX10 is anti-correlated with immune infiltrates and immune-related gene pathways

(A) Melanoma immunohistochemistry (IHC) samples from TCGA (Cancer Genome Atlas Network, 2015) were previously scored for lymphocyte density and lymphocyte distribution. These two scores were summed to give a lymphocyte score. A Spearman's correlation was conducted to determine the relationship between SOX10 mRNA levels and lymphocyte scores.

(B) Gene set enrichment analysis (GSEA) was performed on patient data from the cutaneous melanoma TCGA dataset to determine the relationship between SOX10 mRNA levels and Kyoto Encyclopedia of Genes and Genomes (KEGG) gene pathways. Shown are the pathways significantly negatively correlated with SOX10 expression and normalized enrichment scores ($p < 0.05$). In bold are immune-related pathways.

(C) Shown are enrichment plots, related to (B).

KEY RESOURCES TABLE

REAGENT or RESOURCE	SOURCE	IDENTIFIER
Antibodies		
SOX10	Cell Signaling	D5V9L; RRID:AB_2792980
SOX10	Santa Cruz	A-2; RRID:AB_10844002
CEACAM1	Cell Signaling	D1P4T; RRID:AB_2798605
CEACAM1	R&D Systems	Polyclonal; #AF6480; RRID:AB_10718854
ACTIN	Sigma	A2066: RRID:AB_476693
TYROSINASE	Abcam	ab61294; RRID:AB_946016
GP100	Abcam	ab137078; RRID:AB_2732921
MELAN-A	Abcam	ab210546; RRID:AB_2889292
MITF	Cell Signaling	D5G7V; RRID:AB_2616024
ZEB1	Cell Signaling	E2G6Y; Catalog no. 70512T
CD47	Cell Signaling	D3O7P; RRID:AB_2799637
CEACAM1	BioLegend	mAb-CC1; RRID:AB_2632799
CEACAM1	R&D Systems	283340: RRID:AB_2077348
HVEM	BioLegend	HMHV-1B18; RRID:AB_2303381
HVEM	BioLegend	122; RRID:AB_2565472
PD-L1	BioLegend	Clone 10F.9G2; RRID:AB_2563635
CD47	BioLegend	miap301; RRID:AB_2629538
CD47	BioLegend	CC2C6; RRID:AB_2721547
Galectin-9	BioLegend	RG9-35; RRID:AB_2562296
CD45.2	BioLegend	Clone 104; RRID:AB_10900256
CD3	BioLegend	Clone 17A2; RRID:AB_2621731
CD8α	BioLegend	Clone 53-6.7; RRID:AB_11124344
CD8β	BioLegend	YTS156.7.7; RRID:AB_2260149
Armenian Hamster IgG isotype control	BioLegend	HTK888; Catalog no. 400912
Mouse IgG1, κ isotype control	BioLegend	MOPC-21; RRID:AB_893664
Mouse IgG2b, κ isotype control	BioLegend	MPC-11; Catalog no. 400313
CD8α	BioXCell	53-6.72; RRID:AB_1107671
Rat IgG2a	BioXCell	2A3; RRID:AB_1107769
Chemicals, peptides, and recombinant proteins		
IFNγ	R&D Systems	285-IF-100
Critical commercial assays		
RNeasy Plant Mini Kit	QIAGEN	74904
Deposited data		
YUMM1.1 CRISPR SOX10 RNA-seq	This paper	BioProject ID: PRJNA688784
MeWo CRISPR SOX10 RNA-seq	C.C., unpublished data	BioProject ID: PRJNA701949

REAGENT or RESOURCE	SOURCE	IDENTIFIER
ATAC-seq SOX10 knockdown	PMID: 25516281	GEO DataSets: GSE114557
Experimental models: Cell lines		
Human: MeWo Melanoma Cell line	Case Western Reserve	MeWo
Human: SKMel28 Melanoma Cell Line	ATCC	SKMel28
Human: SKMeL30 Melanoma Cell Line	Memorial Sloan Kettering Cancer Center	SKMel30
Mouse: YUMM1.1 BRAF V600E Melanoma Cell Line	Yale University	YUMM1.1
Mouse: B16F10 Melanoma Cell Line	ATCC	B16F10
Mouse: 1014 Melanoma Cell Line	Institut Curie, Orsay, France	1014
Experimental models: Organisms/strains		
Mouse: C57BL/6 Mice	Jackson Labs	C57BL/6
Mouse: NOD.*Cg-Prkdc^{scid}Il2rg^{tm1Wjl}/SzJ*	Jackson Labs then bred at Thomas Jefferson University	NSG
Mouse: B6.129S7-Rag1tm1Mom/J	Jackson Labs then bred at Thomas Jefferson University	RAG1 KO
Oligonucleotides		
SOX10 siRNA #1	Dharmacon Inc.	D-017192-01
SOX10 siRNA #2	Dharmacon Inc.	D-017192-02
SOX10 siRNA #3	Dharmacon Inc.	D-017192-03
Non-targeting CTL siRNA	Dharmacon Inc.	D-001810-01
SOX10 crRNA #1	Dharmacon Inc.	CM-049957-01-0002
CEACAM1 crRNA #1	Dharmacon Inc.	CM-055898-01-0002
Recombinant DNA		
pLenti4/TO/mHVEM	Generated by S. Rosenbaum	N/A
pLentihygro/mSOX10-noV5	Generated by S. Rosenbaum	N/A
pLentihygro/TO/GW/GFP	Generated in Aplin lab	N/A
pLentiPuro3/TO/GW/emGFP	Generated in Aplin lab	N/A
pLentiPuro3/TO/GW/hSOX10	Generated in Aplin lab	N/A
pDONR221-SOX10	Addgene	#24749
Software and algorithms		
FlowJo	FlowJo, LLC	N/A
Quantity One	BioRad	N/A
Graphpad Prism	GraphPad	N/A
Integrated Genome Viewer (IGV 2.8.6) program	Broad Institute	N/A
IncuCyte® software	Essen Biosciences	N/A
R project	N/A	http://www.R-project.org